p. 1

Papers Presented to the International Colloquium on Venus

N93-14289 484159

VENUS RADAR MAPPING FROM THE VENERA 15 AND 16 SPACECRAFTS: RESULTS AND RESTRICTIONS. E. L. Akim[1], A. I. Zakharov[2], and A. P. Krivtsov[2], [1]Institute of Applied Mathematics, Russian Academy of Sciences, Russia, [2]Institute of Radioengineering and Electronics, Russian Academy of Sciences, Russia.

This report contains a description of the results of the Venus northern hemisphere radar survey in 1983–1984 from the Venera 15 and 16 spacecrafts. In addition, we discuss some peculiarities in the function of the radar equipment that defined the technology of SAR data processing. Among these peculiarities are insufficient calibration of SAR and radar altimeter and erroneous automatic gain control data transmission from the spacecrafts.

As a result, the procedure of image synthesis and mosaicking contained multistage image brightness corrections. This led to the fact that the average image brightness in a spot 100 km in diameter was constant everywhere in the mosaics.

Twenty-seven radar mosaics in the Lambert-Hauss conic projection with 1–2-km spatial resolution covering 25% of the surface of Venus have been produced.

A Venus surface roughness map was constructed by joint processing of SAR and altimeter data. The mutual calibration of the SAR and altimeter was made in the special radar session, when the SAR and altimeter were declined from the local vertical at the same angle.

The possibility of estimating relative variations in surface reflection properties over a tens-of-kilometers interval from Venera images is still being considered.

Joint analysis of the coordinates of small features on the Venera and Magellan images is one more approach being used to refine the period of rotation for Venus.

484160

N93-14290

LOCAL-TIME ASYMMETRIES IN THE VENUS THERMOSPHERE. M. J. Alexander[1], A. I. F. Stewart[1], and S. W. Bougher[2], [1]Laboratory for Atmospheric and Space Physics, University of Colorado, Boulder CO 80309, USA, [2]Lunar and Planetary Laboratory, University of Arizona, Tucson AZ 85721, USA.

Our current understanding of the global structure and dynamics of the Venus thermosphere is embodied in models such as the Venus Thermospheric General Circulation Model (VTGCM, [1]) and empirical composition models such as VIRA [2] and VTS3 [3]. To first order the thermosphere is symmetrical about the axis through the subsolar and antisolar points. Solar radiation at extreme ultraviolet and infrared wavelengths heats the dayside thermosphere and drives a subsolar-to-antisolar (SS-AS) circulation pattern with strong winds (250–300 m/s) across the terminator. This circulation advects low mass atoms (H and He) and heat from the dayside to the nightside. The forcing provided by the solar heating is strong, such that the VTGCM has had to include a prescribed wave drag term to slow the winds and match diurnal variations in temperature and O and CO.

This simple symmetric picture is modified by a thermospheric "superrotation," i.e., the thermospheric winds also have a westward (in the same direction as the lower atmosphere rotation) zonal component with a magnitude of approximately 50–75 m/s. Since the thermospheric winds have never been measured directly, this has been inferred from nightside density and nightglow distributions that have been associated with the nightside convergence point of the SS-AS circulation. Hydrogen and He peak in density on the nightside, but not at the antisolar point. Their density peaks are shifted into the early morning hours at 5 a.m. and 3 a.m. respectively. Nightglow emissions from NO that are also associated with the antisolar convergence of the winds have been observed to peak at 2 to 3 a.m. local time. The current VTGCM includes this superrotation with an asymmetric Rayleigh drag prescription.

We have completed an analysis of ultraviolet images of Venus at 130 nm acquired by the Pioneer Venus Orbiter Ultraviolet Spectrometer (PVOUVS). This emission originates from oxygen atoms in the Venus thermosphere. Oxygen is one of the main constituents at these altitudes, and so with careful modeling we can infer important information about the structure of the thermosphere from these data. *In situ* measurements of thermospheric densities [4] were only accomplished at low latitudes and near the maximum in solar activity, while the PVOUVS images show latitudes from 60°S to the north pole and now span an entire solar activity cycle. We have examined 97 images spanning the 10-year period between 1980 and 1990, and have developed a technique for global radiative transfer modeling with which we create synthetic models of each image analyzed [5,6]. The models incorporate our current understanding of the thermosphere described above. We study the ratio of data and model images to remove observational geometry artifacts. In these ratio images we have found a persistent pattern in 130-nm brightness that is present in every image analyzed. It appears as an asymmetry in local time with lowest values at the morning terminator and relatively high values in the late afternoon. To examine the average structure of these patterns, we map each ratio image into latitude and local time, and average them to create a map of solar-locked features. Figure 1 shows the result. We can relate these solar-locked brightness patterns directly to variations in atomic oxygen, and find that the a.m. to p.m. densities differ by up to a factor of 2 where the VTGCM predicts only a 5% variation. The asymmetry is present only at latitudes poleward of 30°, and so was not observed in the *in situ* measurements taken at equatorial latitudes.

We have developed a hypothesis for understanding the persistent local-time asymmetry observed in Fig. 1 as a signature of vertically propagating internal gravity waves interacting with the thermospheric SS-AS cirulation. If the source for these waves is presumed to be in the upper cloud deck or just above, and if they saturate in the thermosphere, they will create a striking asymmetry in eddy diffusion with local time. Experiments we have conducted with the VTGCM suggest that such variations in eddy diffusion can account for the oxygen variations we observe in the PVOUVS data. We use a parameterization first developed by Lindzen [7] to study variations in eddy diffusion with local time. The magnitude of the eddy diffusion K is a strong function of the difference between the mean zonal wind speed and the phase speed of the wave,

$$K \propto |\bar{u} - c|^4$$

So waves with predominantly westward phase speeds—like those forced in the upper clouds—will interact very differently with the

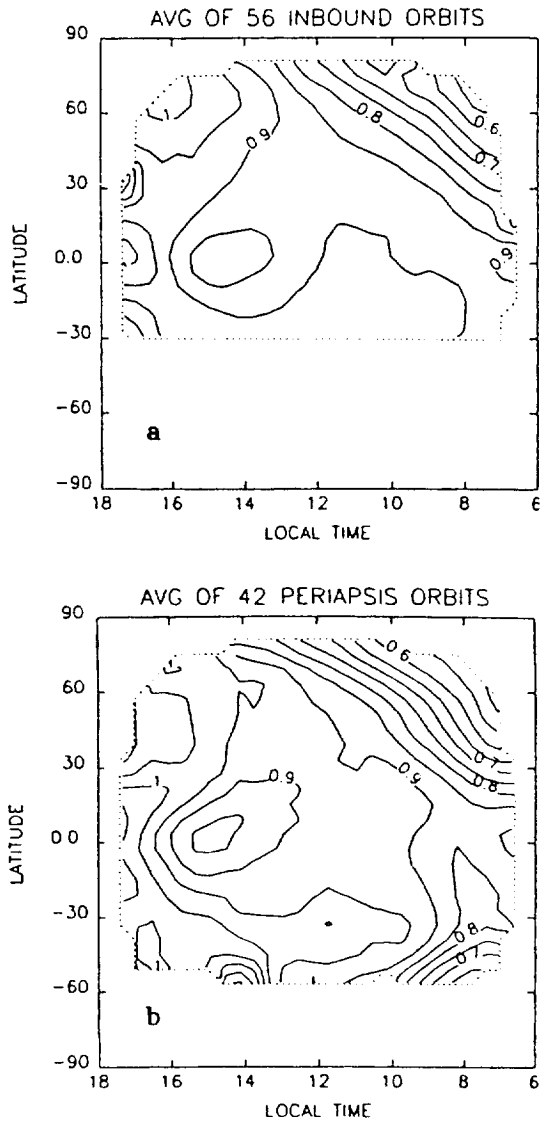

Fig. 1. Contours of brightness ratio (data/model) of the 130-nm emission displaying the local-time asymmetry (see text). The brightness ratio patterns can be thought of as anomalous patterns in O. (a) and (b) are derived from two different types of PVOUVS data: (a) contains more data, so it better displays the northern hemisphere pattern, but in (b) we can see to more southerly latitudes. The northern hemisphere pattern is mirrored there.

westward afternoon winds than with the eastward morning winds. Figure 2 shows some example eddy diffusion profiles calculated with this method. Early morning a.m. values are typically a factor of 10 or more larger than corresponding p.m. values. These local-time asymmetries will be discussed in more detail in the context of several scenarios for the middle atmosphere wave forcing. This same mechanism can also give rise to asymmetric wave drag forces that have the potential for generating the thermospheric superrotation. The mechanism for *in situ* forcing of the thermospheric superrotation is still considered a mystery, so this corollary provides strong support to our cloud-level wave source hypothesis.

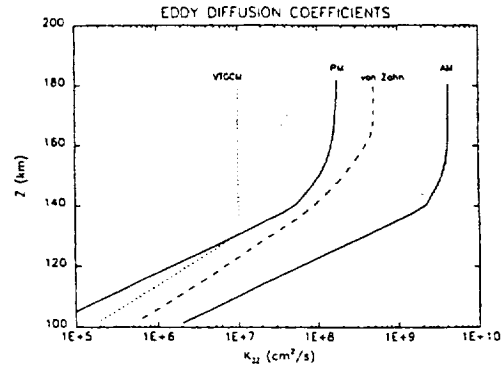

Fig. 2. Eddy diffusion coefficients characteristic of 8 a.m. and 4 p.m. wind profiles derived with the Lindzen parameterization [7]. Also shown are the VTGCM and von Zahn et al. [8] one-dimensional photochemical model *K* for reference.

References: [1] Bougher et al. (1988) *Icarus, 73*, 545–573. [2] Keating et al. (1986) *Adv. Space Res., 5*, 117–171. [3] Hedin et al. (1983) *JGR, 88*, 73–83. [4] Niemann et al. (1980) *JGR, 85*, 7817–7827. [5] Meier R. R. and Lee J.-S. (1982) *Planet. Space Sci., 30*, 439–450. [6] Alexander et al. (1991) *Bull. AAS, 23*, 1194. [7] Lindzen R. S. (1981) *JGR, 86*, 9707–9714. [8] von Zahn et al. (1980) *JGR, 85*, 7829–7840.

N93-14291

RINGED IMPACT CRATERS ON VENUS: AN ANALYSIS FROM MAGELLAN IMAGES. Jim S. Alexopoulos and William B. McKinnon, Department of Earth and Planetary Sciences and McDonnell Center for the Space Sciences, Washington University, St. Louis MO 63130, USA.

We have analyzed cycle 1 Magellan images covering ~90% of the venusian surface and have identified 55 unequivocal peak-ring craters and multiringed impact basins. This comprehensive study (52 peak-ring craters and at least 3 multiringed impact basins) complements our earlier independent analysis of Arecibo and Venera images and initial Magellan data [1,2] and that of the Magellan team [3].

Peak-ring craters are characterized by an outer, well-defined radar-bright rim, and an inner bright ring defined by a concentric arrangement of isolated and sometimes clustered peaks. The general appearance of venusian peak-ring craters, including their inner rings and crater rims, is morphologically similar to equivalent structures on the Moon, Mars, and Mercury. Some venusian peak rings, however, are distorted in shape (noncircular outline of inner ring) and off-center. Ejecta morphologies around peak-ring craters vary from regular and symmetric, including those due to oblique impact, to irregular and asymmetric. Many peak-ring craters exhibit outflow channels. The outflows emanate from within the crater and breach the crater rim (e.g., Cleopatra), while others extend away from the distal end of the ejecta blanket or have been incorporated within the main ejecta deposit (e.g., Cochran). The interiors of most peak-ring craters are radar-dark or smooth (similar to surrounding plains), although some are bright. A few larger craters are completely flooded and show no interior structure or inner ring (e.g., Koidula, ~70 km in diameter, and Alcott, ~65 km in diameter). The radar-smooth signature of the interior is likely due to postimpact resurfacing, either volcanism or (possibly differentiated) impact